AGU ADVANCING EARTH AND SPACE SCIENCES

Earth and Space Science

RESEARCH ARTICLE
10.1029/2024EA003703

Long Period Seismology on Titan in the Presence of a Methane Clathrate Lid

Andrea S. Bryant[1,2], **Mark P. Panning**[2], **and Angela G. Marusiak**[3]

[1]University of Chicago, Department of Physics, Chicago, IL, USA, [2]Jet Propulsion Laboratory, California Institute of Technology, Pasadena, CA, USA, [3]University of Arizona, Lunar and Planetary Laboratory, Tucson, AZ, USA

Key Points:

- Based on simulations, the Rayleigh wave signal is dominated by the first overtone at frequencies >20 mHz
- Given likely measurement uncertainty, it is unlikely that we can resolve clathrate layers in thick ice shells of icy ocean worlds
- We resolve the frequency range of flexural waves transitioning to a Stoneley wave (mode) in the fundamental mode

Supporting Information:

Supporting Information may be found in the online version of this article.

Correspondence to:

A. S. Bryant,
asbryant@uchicago.edu

Citation:

Bryant, A. S., Panning, M. P., & Marusiak, A. G. (2024). Long period seismology on Titan in the presence of a methane clathrate lid. *Earth and Space Science*, *11*, e2024EA003703. https://doi.org/10.1029/2024EA003703

Received 26 APR 2024
Accepted 8 NOV 2024

Author Contributions:

Conceptualization: Andrea S. Bryant, Mark P. Panning, Angela G. Marusiak
Data curation: Andrea S. Bryant
Formal analysis: Andrea S. Bryant
Funding acquisition: Mark P. Panning
Investigation: Andrea S. Bryant
Methodology: Andrea S. Bryant, Angela G. Marusiak
Resources: Mark P. Panning
Software: Mark P. Panning
Supervision: Mark P. Panning
Validation: Angela G. Marusiak
Writing – original draft: Andrea S. Bryant

Abstract Previous 1-D spherically symmetric seismic modeling studies have shown that in the presence of a clathrate lid on Titan significant thermal profile differences result, particularly in comparison to a pure water ice shell. In turn, these thermal differences would lead to notable changes in the waveform amplitudes and seismic phase arrival times. In this study we investigate the feasibility of using surface waves dispersion to explore the structure of Titan's ice shell. We investigate the ability to measure and observe the frequency-dependent signals (0.003–0.100 Hz) and their utility in being able to detect existence of a methane-clathrate lid. We find that we are unlikely to resolve the clathrate-lid's existence using long-period techniques, and this could be a limitation for studying very thick ice shells ($> \approx 20$ km) of icy ocean worlds. We did resolve the frequency range of flexural waves transitioning to a Stoneley wave (mode) in the fundamental mode, and see a Rayleigh wave in the first overtone for a 100 km ice shell on Titan for a simulated quake.

1. Introduction

Titan is of much interest as it is one of the largest moons in the Solar System and contains both an atmosphere and a subsurface ocean. On its surface there are sand dunes of organic material and methane lakes. The ice shell is thought to be 45–120 km thick (Deschamps et al., 2010; Durante et al., 2019; Mitri & Showman, 2008; Vance, Panning, et al., 2018), and beneath the thick ice is an ocean greater than 80 km in depth (Grasset et al., 2000; Sohl et al., 2003; Sotin et al., 2021; Stähler et al., 2018). Seismology is a potentially powerful tool that may uncover many of Titan's secrets including but not limited to; the ocean depth and chemistry, ice thickness, presence or lack thereof of high-pressure ice phases, and silicate interior properties. Insights into these scientific parameters have broader implications for studies of astrobiology and habitability of the Titan system, especially given Titan's unique surface conditions (being the only body beyond Earth in the Solar System to currently have long-lasting liquid on its surface) (Stofan et al., 2007; R. M. Lopes et al., 2007; Hayes, 2016).

Much knowledge about Titan has been obtained from data from the *Cassini–Huygens* mission to the Saturnian system (R. M. C. Lopes et al., 2019; Hayes et al., 2018; Lebreton et al., 2009)). Using Schumann resonance, the first direct estimates of the ice shell were given: 55–80 km, in line with earlier internal structure models (Béghin et al., 2012; Lorenz & Le Gall, 2020; Sohl et al., 2003; Tobie et al., 2005). However, investigations from *Cassini–Huygens'* electric field, geophysical, and gravitational data suggest that Titan's ice shell could be anywhere from 25 to 200 km thick (Baland et al., 2014; Béghin et al., 2012; Deschamps et al., 2010; Durante et al., 2019; Hemingway et al., 2013; Iess et al., 2012; Mitri & Showman, 2008; Nimmo & Bills, 2010; Sohl et al., 2014; Tobie et al., 2006). Due to Titan's high gravitational moment of inertia factor (0.341, Durante et al., 2019), a metallic core is not expected from compositional models (Vance, Panning, et al., 2018). A diverse abundance of organics have been shown to be present in Titan's surface and atmosphere, from *Cassini–Huygens* and Earth-based measurements (Barnes et al., 2021; Cordiner et al., 2015, 2018; Hörst, 2017; Janssen et al., 2016; Lai et al., 2017; Niemann et al., 2005; Nixon et al., 2020; Thelen et al., 2019, 2020). In particular, organics created in the atmosphere can settle over Titan's bedrock composed of water–ice (Barnes et al., 2021; Rodriguez et al., 2006; Barnes et al., 2007; Soderblom et al., 2007; Le Mouélic et al., 2008; Janssen et al., 2009, 2016; Hayne et al., 2014; Neish et al., 2015; R. M. C. Lopes et al., 2019).

Since the *Huygens* probe was only able to directly image Titan's surface and give rough estimates of the interior structure, many questions remain outstanding (Elachi et al., 2005; Iess et al., 2014; Marusiak et al., 2021; Porco et al., 2006). For example, the dynamics and internal structure of the ice shell are still not well understood (Carnahan et al., 2022; Marusiak et al., 2021). However the use of a geophysical suite including seismic instrumentation may uncover key unknowns about Titan in the coming decades (i.e., the *Dragonfly* mission)

Writing – review & editing: Andrea S. Bryant, Mark P. Panning, Angela G. Marusiak

Table 1
Mode (n) and Wavelength Dependence of Waves for a 100 km Thick Ice Shell Under Titan-like Conditions, Following Panning et al. (2006) and Stähler et al. (2018).

Mode (n)	d & λ	Wave Type	v_p, v_g & f
0	$\lambda > 2\pi d$	Flexural wave (entire ice shell)	$v_g = 2v_p$ $v_g \propto \sqrt{f}$
0	$d < \lambda < 2\pi d$	Transition between flexural and Stoneley wave	
0	$\lambda < d$	Stoneley wave (ocean/ice shell interface)	$v_p = 0.87 v_{\bar{P},ocean}$
1	$\lambda < d$	Rayleigh wave (surface, non-dispersive)	$v_g = v_p$

Note: Variables: d = Ice Shell Thickness, λ = Wavelength of Surface Wave, v_p = Phase Velocity, v_g = Group Velocity, f = Frequency, $v_{\bar{P},\text{ocean}}$ = P-Wave Velocity of the Ocean. Here, $n = 0$ Corresponds to the Fundamental Mode Branch, and $n = 1$ Corresponds to the First Overtone.

(Lorenz et al., 2018; Turtle & Lorenz, 2021). To investigate various aspects of Titan, much work has been done using the data from *Cassini–Huygens*, and much more work remains ongoing in preparation for the upcoming *Dragonfly* mission. The main expected sources of seismic events are thought to be ice cracking driven by the tidal cycles of Titan from Saturn (Marusiak et al., 2021; T. Hurford et al., 2020), although there remains a number of other potential seismic sources, for example, active cryovolcanoes hidden beneath the ice (Schurmeier et al., 2023). Both the hydrocarbon lakes and atmosphere of Titan will also contribute background seismic noise, similar to Earth's background seismic noise due to Earth's oceans and atmosphere (Dybing et al., 2019; Gutenberg, 1947; Stähler et al., 2019).

NASA's *Dragonfly* mission is currently scheduled to launch in 2028 and land on Titan in the mid-2030s. *Dragonfly* is largely an astrobiological mission, with the search for prebiotic chemistry as an overarching theme of its mission goals (Barnes et al., 2021; Lorenz et al., 2018; Turtle & Lorenz, 2021). Its target landing site is near the Selk crater (80 km diameter), a location where liquid water once mixed with surface organics (Barnes et al., 2021; Lorenz, MacKenzie, et al., 2021). The rotorcraft itself is a dual-quadcopter that will hold many astrobiology-focused instruments, including the DraGMet (*Dragonfly* Geophysics and Meteorology) instrument package, containing a seismometer and two geophones to measure seismicity (Barnes et al., 2021; Lorenz, Shiraishi, et al., 2021).

Seismology is a robust tool that will reveal details of interior structures of planets where it otherwise would have been difficult or non-unique. Seismometers were placed on the Moon during the Apollo landings and measured thousands of deep and shallow moonquakes that revealed secrets of the lunar interior (Nakamura et al., 1982; Nunn et al., 2020, 2022). Additionally, data from the *InSight* lander revealed the interior of Mars including the core, crust and upper mantle compositions (Banerdt et al., 2020; Khan et al., 2021; Knapmeyer-Endrun et al., 2021; Stähler et al., 2021). More plans are in the works for what we can learn about the Solar System bodies from seismology (Sun et al., 2023).

It has been argued that seismology is the preeminent tool to determine "vital signs" on icy ocean worlds (Marusiak et al., 2021; Vance, Kedar, et al., 2018). Unlike Earth, where rock is the primary medium in the crust, ice is the dominant surface material on these bodies. There are specific seismic phases that are distinct to ocean world environments (e.g., flexural and Crary waves). On Earth, Love and Rayleigh waves dominate surface wave observations.

One of the most significant parameters for characterizing icy ocean worlds, that could be constrained via direct seismic measurements of the surface, is the thickness of the ice shell. Initial constraints on this observation can be derived from body wave measurements based on *P* and *S* reverberation timing within the ice shell, in addition to the depth dependent epicenter. The ice thickness may be further constrained using the characteristic harmonic frequency of the Crary wave and the recovered *P*- and *S*-wave velocities in the ice. Panning et al. (2006) also proposed that surface waves (longer period waves than body waves (*P* and *S* waves), for example, Love, flexural, and Rayleigh waves) may be a good tool for estimating ice shell thickness, as the fundamental mode Rayleigh wave has a characteristic group velocity maximum associated with a transition from a flexural wave at low frequencies to something more similar to a Rayleigh wave in a half-space at higher frequencies (Table 1). In this study we see that transition zone between 2.1 to 13.7 mHz, for a 100 km Titan-like ice shell.

Methane-clathrates (cage-like carbon molecules which encase methane) are thought to readily form under Titan-temperatures and pressures. Because of this, it is thought that the surface of Titan could contain tens of kilometers of clathrates that could potentially be detectable with seismology, particularly due to the differences in thermal conductivities between water ice and methane-clathrates (Choukroun et al., 2010; Hand et al., 2006; Helgerud et al., 2003, 2009; Lunine & Stevenson, 1985, 1987; Waite et al., 2007). This study explores the use of long-period seismic wave dispersion of surface waves (e.g., Love, Flexural, Rayleigh, etc.) as a means to learn more about Titan's interior. In particular we focus in this study on determining if it is feasible to distinguish between the various clathrate models (no clathrate, 10 and 20 km clathrate lid) using this method. The phase and group velocities are both dependent on the frequency. Because dispersion is related to the properties of the medium, the *Dragonfly* seismometer may record surface wave dispersion to explore Titan's interior. Due to the Rayleigh surface wave being a prominent feature of the seismograms for a simulated quake, we will focus on measuring Rayleigh wave group velocities. We only investigate the vertical component as the *Dragonfly* seismometer is only sensitive in the vertical component (Lorenz, MacKenzie, et al., 2021). There are expected to be horizontal component geophones on *Dragonfly*, but the sensitivity will be lower while the noise is expected to be higher (Lorenz, Shiraishi, et al., 2021). Given the expected limitations of *Dragonfly* seismic data, we have chosen to focus on the simplest approaches to measuring surface wave velocity dispersion rather than employing methods requiring detailed waveform modeling and high signal-to-noise ratios, but such methods may be explored if large and clear events are observed by *Dragonfly*. In the case of icy ocean worlds, surface Rayleigh waves are shorter period waves (compared to flexural waves) that don't interact with the bottom of the ice shell (Table 1) and can be described with the usual retrograde elliptical motion, as seen on Earth. In contrast to Rayleigh waves that only see the top of the ice shell, longer period flexural waves are full-layer, or affect the entire depth of the ice shell. However, they are only seen at low frequencies. In this study, Rayleigh waves are the prominent surface wave (Table 1) at >14 mHz and above. It is also important to note that the velocity gradient is very small with depth, so Rayleigh waves have very little dispersion in ice shells (Stähler et al., 2018). While the high scattering environment of Earth's Moon has limited surface wave observations and modeling, such approaches have been critical in increasing our understanding of the interior of Mars (Beghein et al., 2022; Drilleau et al., 2023; Kim et al., 2022, 2023; Li et al., 2022; Panning et al., 2023) and has long been proposed for use on Europa and other icy ocean worlds (Kovach & Chyba, 2001; Marusiak et al., 2023; Panning et al., 2006; Stähler et al., 2018).

This method of using long period seismology has been particularly useful to study other planetary bodies besides Earth: to constrain elements of the Martian interior: Kim et al., 2023 and 2022, Panning et al., 2023, Beghein et al., 2022, etc.); there are not so many examples for the Moon but Dal Moro et al., 2023 provides a notable study, and also a similar study to this work in particular was performed for Europa in 2006: Panning et al., 2006. Thus this work is not done in isolation, but apart of a growing number of extaterrestial synthetic seismology studies. In the absence of real data, synthetic seismic profiles serve as a baseline for comparing real seismic data to. This type of approach was used for Mars *InSight* seismology—they created a large catalog of potential events (≈ 5000) and were able to use that catalog to figure out what the events they were seeing were. This case study is just one such event in ongoing effort to catalog potential titanquake profiles in preparation for the *Dragonfly* mission.

2. Methods

We use two models from Marusiak et al. (2022) including one with no clathrates and one with a 10 km clathrate lid integrated according to the numerical results of Kalousová and Sotin (2020). Kalousová and Sotin (2020) provide the thermal profiles for a conductive stagnant lid on top of a convective ice layer on Titan. The results from their numerical simulations of thermal convection on a 100 km ice shell informs the ice shell models of Marusiak et al. (2022) and this work. Marusiak et al. (2022) demonstrated large changes in seismic ground motions and arrival times (≤2.0%) when comparing the 10 km-thick methane clathrate lid to an ice shell of water ice. In this study we have modeled a 20 km-thick clathrate lid as well. We choose not to vary the overall ice shell thickness, though, as implications of that have been discussed in other papers (Marusiak et al., 2023; Panning et al., 2006; Stähler et al., 2018) and the impact of that on long-period surface waves has been well-characterized, while this study is focusing on whether variations in the thickness of a potential surface clathrate layer would be resolvable in long-period seismic data. The three models chosen (no clathrate layer, 10 and 20 km) cover the range of reasonable models of stable clathrate layers that could be maintained without being mixed into the ice shell through convection. A shallow source depth is chosen because cracking events are more likely in the cold and brittle upper portion of the ice shell, and shallow sources maximize surface wave energy which we are analyzing

in this study. Magnitude 3 (M_w =3) events are a reasonable expectation for events that could be observed occurring in each Titan tidal cycle based on a model where seismicity scales with tidal dissipation (T. A. Hurford et al., 2020), but since we are not explicitly including noise levels due to environmental sources and instrument performance, alternative magnitudes can be modeled by scaling. We focus on whether dispersion observations, in a best-case scenario of clear observations of surface waves, can resolve between models of clathrate layer thickness.

Models consist of spherically symmetric interior profiles created with *PlanetProfile* (Styczinski et al., 2023; Vance, Kedar, et al., 2018). *PlanetProfile* creates thermodynamically self-consistent models that match orbital constraints on mass and moment of inertia. In the case of Titan, mass and moment of inertia were measured during the *Cassini–Huygens* mission (Fortes, 2012). The surface temperature was set to 94K (Jennings et al., 2016) and the temperature at the base of the ice shell, (T_b), was approximately 260K for all the models. Model values for T_b are selected to set the ice shell thickness based on the pressure-dependent melting point of the ocean fluid (Journaux et al., 2020). While different ice shell thicknesses will strongly affect the long-period data in icy ocean worlds (Kovach & Chyba, 2001; Marusiak et al., 2021; Panning et al., 2006; Stähler et al., 2018) we chose to look at only one thickness, 100 km, to isolate any specific effects of clathrate layer presence. All ice shells we modeled have a total thickness of 100 km, varying only in thickness of the methane clathrate lid. Only methane-type clathrates were considered for this study as atmospheric methane has been hypothesized to be episodically replenished via outgassing of the methane clathrates present within the top ice layer (Tobie et al., 2006). For this reason it is thought that methane clathrates will insulate Titan's icy shell.

Using the outputted models from PlanetProfile, we then inputted them in the open-source spectral-element code *AxiSEM* (www.axisem.info) to create three-dimensional (3D) global seismic wavefields in an anisotropic, visco-elastic Titan-like media (Nissen-Meyer et al., 2014). In addition, we used *Instaseis,* also open-source (www.instaseis.net) to extract seismograms for arbitrary source–receiver configurations from the databases generated with *AxiSEM* (van Driel et al., 2015). Although originally designed for Earth, *AxiSEM* and *Instaseis* have been adapted for arbitrary spherically symmetric models of other planets and icy ocean worlds. The seismograms were generated for a M_w = 3, double-couple event at 3 km depth. Currently, the exact mechanism of a titanquake has yet to be measured, however double-couple mechanisms do well at representing most sources observed on Earth and planetary bodies, with the exception of impact sources. While the mechanism chosen impacts the relative amplitude of seismic body and surface wave amplitudes, in this study we focus on the general ability of surface wave measurements to differentiate between clathrates models without explicitly taking into account sources of noise in *Dragonfly* measurements, and thus the amplitude has little impact on the study conditions.

Using the output 1D seismic wave velocity profiles from *PlanetProfile* as inputs, dispersion curves and normal modes (eigenfrequencies and eigenfunctions) (Woodhouse, 1988) were computed using a version of the code *Mineos* (Masters et al., 2011; Panning et al., 2018) (Figure 1). This code also computes synthetic seismograms using normal mode summation in a spherically symmetric planetary model. The complete seismogram of Titan can be expressed as a sum of the normal modes, with the proper corresponding excitation factors, similar to normalization coefficients (Shearer, 2019). Eigenfunctions for an given eigenfrequency can be written as

$$u(r) = \left[{}_nU_l(r)e_r + {}_nV_l(r)\nabla_1 - {}_nW_l(r)(e_r \times \nabla_1)\right] Y_l^m(\theta,\phi), \tag{1}$$

where n is the radial order, l the angular order, m the azimuthal order, and Y_l^m is the spherical harmonic (variables defined in Table 2). Normal modes were generated considering both spheroidal and toroidal dispersion data (Masters et al., 2011). As mentioned in introduction section, this study presents theoretical dispersion curves generated for spheroidal modes, in accordance with the sensitivity specifications that *Dragonfly's* DraGMet seismometer will have (being sensitive to only the vertical component) (Figures 1 and 2) (Lorenz, MacKenzie, et al., 2021). Under the assumption of radial symmetry, the eigenfrequencies and eigenfunctions are not dependent on l or m, and depend only on radius:

$$\nabla_1 f(\mathbf{r}) = \partial_\theta f(\mathbf{r})\mathbf{e}_\theta + (\sin\theta)^{-1}\partial_\phi f(\mathbf{r})\mathbf{e}_\phi, \tag{2}$$

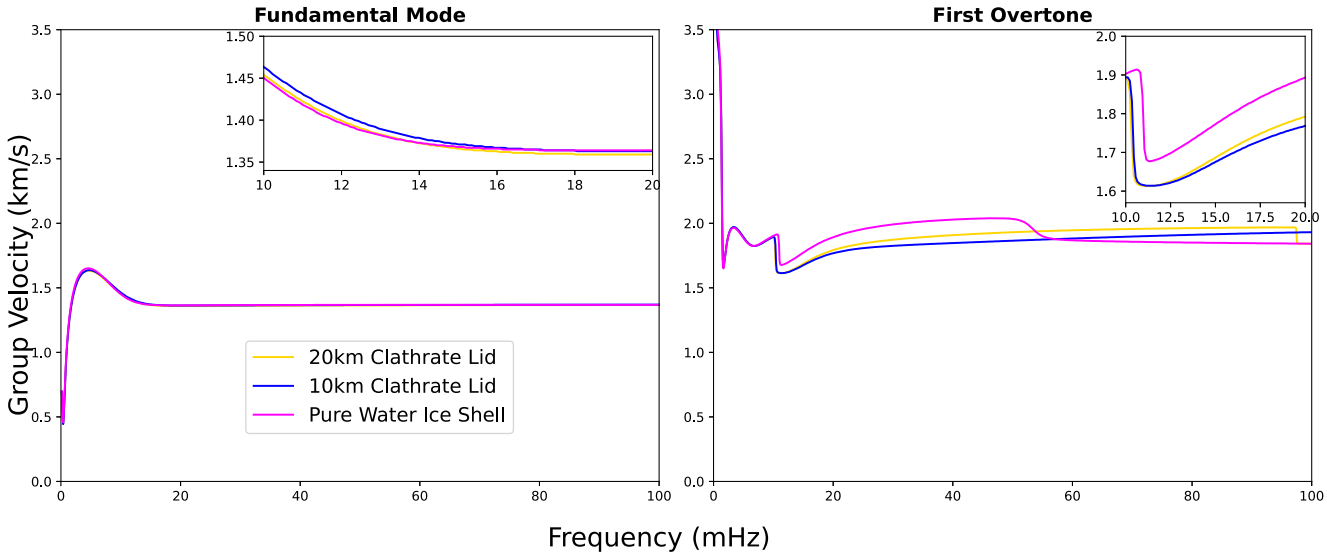

Figure 1. Theoretical dispersion curves, containing group velocity measurements as a function of frequency for all models, produced using *Mineos* v1.0.2 (Masters et al., 2011). Model dependent differences in the group velocities can only be seen in the first overtone, above ≈15 mHz.

with mode normalization

$$\int_0^{r_T} \rho(r)\left({}_nU_l(r) + l(l+1)\,{}_nV_l^2(r)\right) r^2 dr = \int_0^{r_T} \rho(r) l(l+1)\,{}_nW_l^2(r) r^2 dr = 1. \quad (3)$$

where r_T is the radius of the Titan, 2575 km. We look at angular orders up to $l = 3000$, and frequencies up to 150 mHz, although we sample the envelopes at lower frequencies (up to 100 mHz).

Individual overtone modes ($n \geq 0$) were isolated from the normal-mode-summed code in order to identify which mode branch of the Rayleigh wave is dominant. For this reason, we focused mainly on lower-order modes, as the surface-waves are contained in this parameter space, whereas the body waves are contained mainly in the larger-n modes.

We measured group velocity using the seismograms from both methods. This was done to test the validity of comparing *Mineos* and *AxiSEM/Instaseis* since both use different methods of calculating the seismograms; AxiSEM calculated in the time domain, while the normal mode summation is performed in the frequency domain. In order to directly compare the *AxiSEM/Instaseis*-generated seismograms to the full normal-mode-summed seismograms, generated with *Mineos,* we band-pass filtered both between 20 and 100 mHz (Figure 3). Using the *AxiSEM/Instaseis*-generated seismograms, we calculated the group velocities at 25, 50, 75, 100, 125, 150 epicentral distance degrees from the source. For each distance we pick the peaks for 3, 5, 10, 20, 40, 60, 80, 100, and 100 mHz center frequencies, with a 15% edge taper. The seismograms were low-pass filtered at 250 mHz initially, then narrow-band-pass filtered at ±15% of their respective center frequencies (Figure 4).

We also present the results of the envelope picking for observations using the *AxiSEM/Instaseis*-generated synthetic seismograms in comparison with *Mineos* data (Figure 4). In the first panel of Figure 4 we see the mean group velocity measurements (from *AxiSEM/Instaseis*) for the range of the distances and center frequencies, as well 1-σ (standard deviation of the number of samples, normalized to N-1, where N is the number of samples per center frequency) away for each of the three structural models with varying clathrate thicknesses.

Table 2
Definitions of Major Terms From Equations 1–3 Used for Calculating Theoretical Dispersion Curves as Well as the Normal Modes (Woodhouse, 1988; Masters et al., 2011; Panning et al., 2018)

Variable	Definition
r, r_T	radius, Titan radius
n	radial order
l	angular order
ρ	density
m	azimuthal order
$f(r)$	eigenfrequency
${}_nW_l(r)$	toroidal eigenfunction
${}_nU_l(r)$, ${}_nV_l(r)$	spheroidal eigenfunctions
$Y_l^m(\theta, \phi)$	spherical harmonics

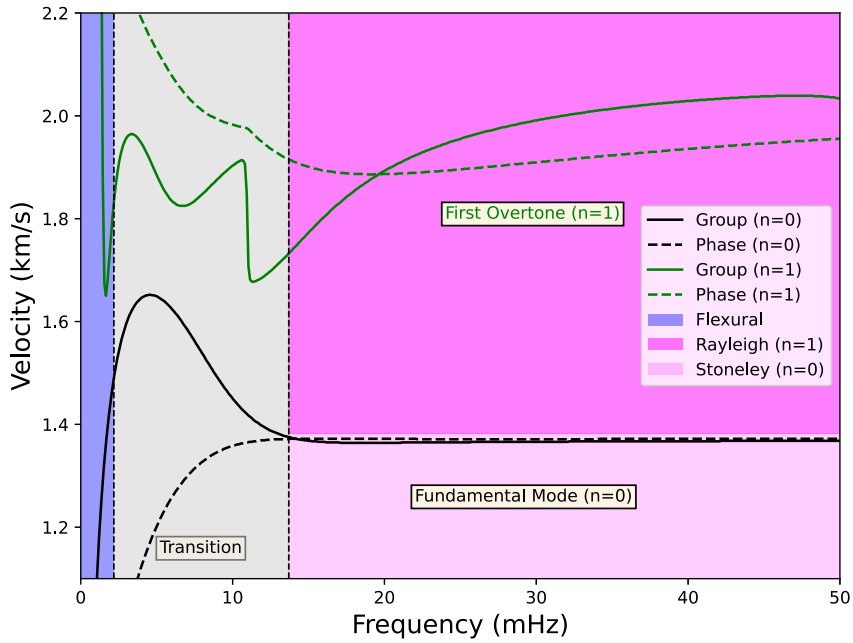

Figure 2. Illustration of the transition between the flexural wave and Stoneley mode in the fundamental mode, and a Rayleigh wave in the first overtone. Group and phase velocities calculated for a Titan model with a 100 km thick ice shell. The transition zone for a 100 km pure water ice shell is between 2.1 and 13.7 mHz. This trend is also the same for the 10 and 20 km methane clathrate lid models.

3. Results

In the fundamental mode, we note that a Stoneley mode (an interface wave propagating at the solid-fluid interface at the base of the ice shell) rather than a Rayleigh mode is dominant for wavelengths less than the thickness of the ice shell, and the flexural wave is dominant for wavelengths greater than $2\pi d$, where d is the thickness of the ice shell (Panning et al. (2006); Stähler et al. (2018), Table 1, Figure 1). While this Stoneley mode behavior of the fundamental mode was not discussed in previous modeling of long-period ocean world seismic wave propagation, for example, (Panning et al., 2006), it is apparent in the modeling of the Titan ice shells due to several factors discussed in this section. In particular, this Stoneley mode behavior can be seen through analysis of the relative amplitudes of the fundamental mode branch and the first overtone, the predicted group velocities of the mode branches, and the shape of the mode eigenfunctions with depth. In the fundamental mode, there is a transitional region between d and $2\pi d$ where the flexural mode transitions to the Stoneley mode. This contribution is partially demonstrated in the normal mode displacement seismograms (Figures 5a–5c and 5e); these seismograms were generated for a $M_w = 3$, double-couple event at 3 km depth so the Stoneley mode is not visible due to both low excitation from a near-surface source, and low amplitudes of the mode for stations on the surface (Figure 6).

We present the theoretical dispersion curves (group velocity as function of frequency) for different modes for the three different interior structure models (Figure 1). The fundamental mode models are nearly indistinguishable from one another, with the group velocity values having the greatest difference of 2.5% for the 10 km and pure water ice shell models, where thermal profiles differ the greatest leading to differences in seismic attenuation and amplitude (Marusiak et al., 2022). For the higher overtones ($n > 0$), group velocities across all models are nearly indistinguishable for frequencies below ≈20–50 mHz. There is considerable frequency dependent group velocity variation above this threshold across the models due to the thermal conductivity-driven seismic attenuation seen in the various thermal lid thicknesses of this study. For moons with thicker ice shells, surface Rayleigh waves are expected to be mostly non-dispersive, thus $v_p \approx v_g$, where v_p is the phase velocity and v_g is the group velocity (Table 1). (Stähler et al., 2018) predicts a characteristic Rayleigh wave velocity of approximately 1.8 km/s, assuming a compression wave velocity ($v_{P,ice}$) of 4 km/s, and a shear wave velocity ($v_{S,ice}$) of 2 km/s, with $v_g \approx v_p = 0.9194\ v_{S,ice}$. We note that the fundamental mode shows a group velocity of 1.4 km/s above the

10.1029/2024EA003703

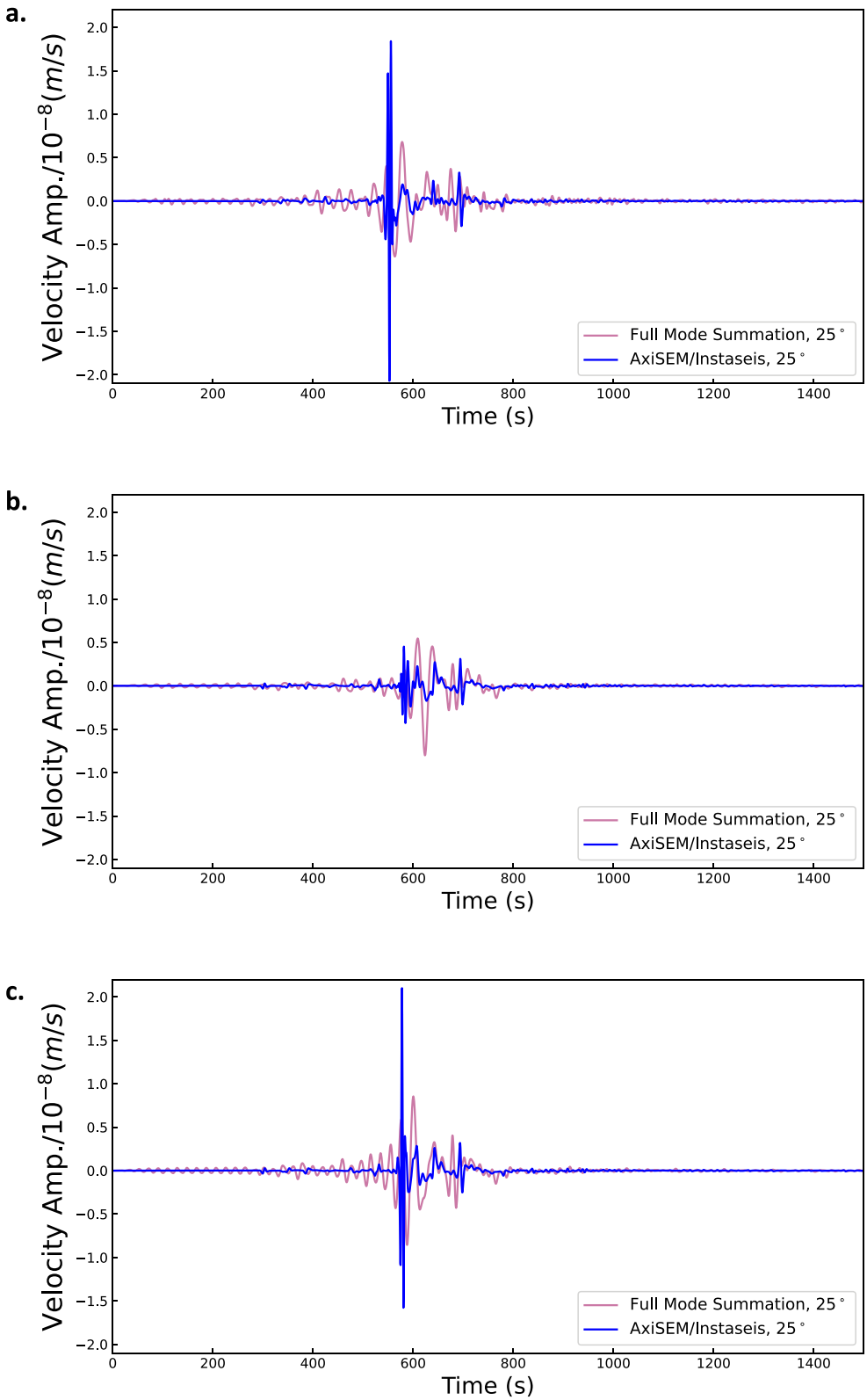

Figure 3. Comparison of band-passed filtered, ground motion velocity seismograms. The seismograms in blue were generated with *AxiSEM/Instaseis*, and the seismograms in were generated via the normal mode summation code *Mineos*: (a) 0 km methane clathrate lid (pure water 100 km ice shell), (b) 10 km methane clathrate lid ice shell, and (c) 20 km methane clathrate lid ice shell. Here the seismograms are in phase, however there is a notable difference in ground motion velocity amplitude between the two-types of seismograms. All seismograms filtered from 20 to 100 mHz.

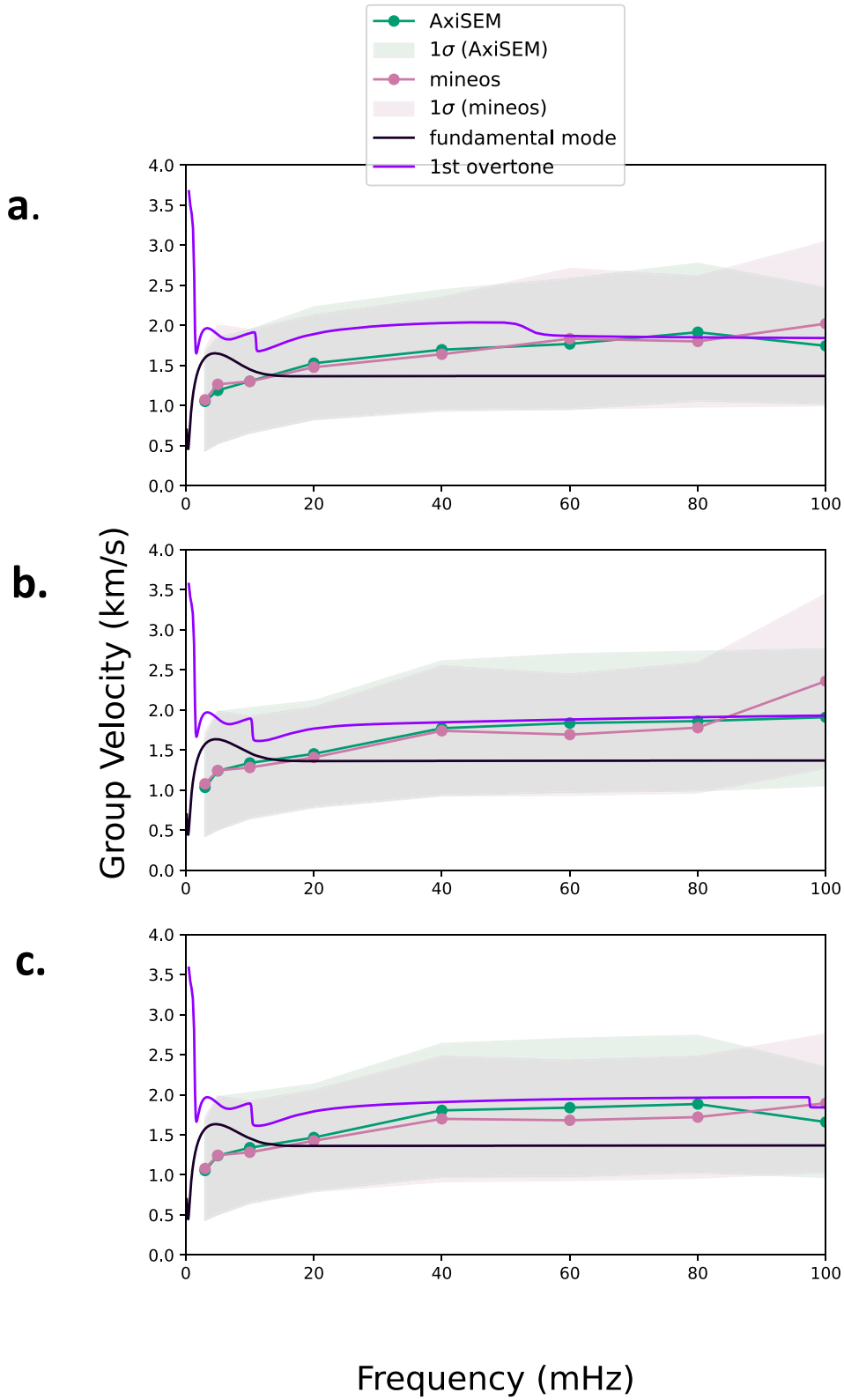

Figure 4.

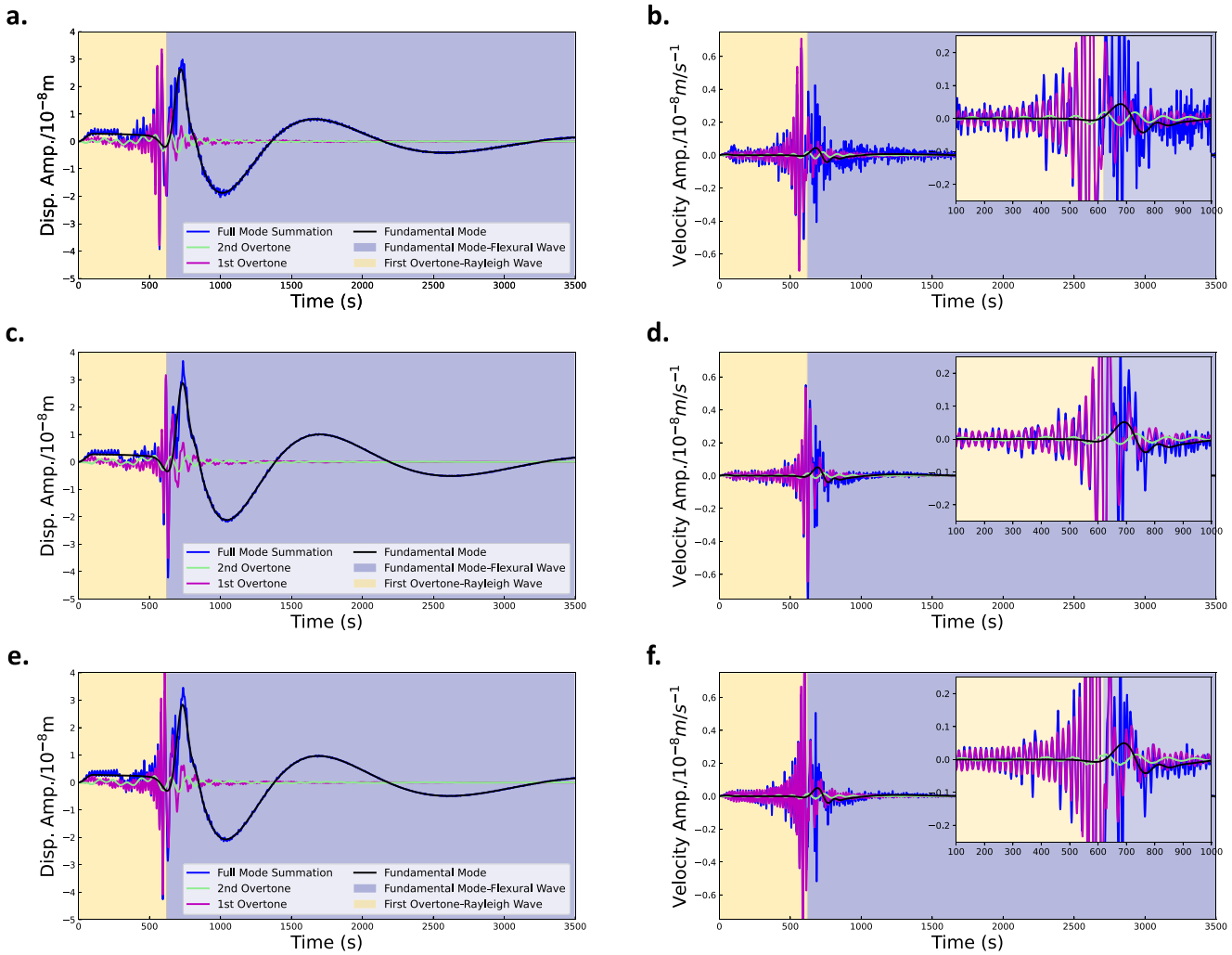

Figure 5. Isolated normal modes generated using *Mineos*, at a distance of 25°. Plotted for all three interior structure profiles, at 3 km depth. The modes plotted include the fundamental mode, as well as overtones 1 to 4. Insets to the right zoom into the fundamental and second overtones as the complete seismogram of summed normal modes up to $n = 999$ is seen to be dominated by the first overtone (a)–(b) 0 km methane clathrate lid (pure water 100 km ice shell) (c)–(d) 10 km methane clathrate lid ice shell, and (e)–(f) 20 km methane clathrate lid ice shell. All models are plotted with displacement (left: (a, c, e), and velocity (right: (b, d, f).

flexural mode, while the first overtone shows a more Rayleigh-like velocity of 1.8 km/s. This provides further support for the interpretation of the fundamental mode as a Stoneley mode, which has a velocity controlled by the P velocity of the underlying ocean (Stähler et al., 2018).

There is overlap of the $\pm 1\sigma$ region for either method with the fundamental mode, especially below ≈20 mHz for calculated group velocities from the mean times given from the peak of the envelopes of the narrow filtered data. However, it is important to note that various interior models are indistinguishable from each other based upon using dispersion measurement techniques alone. The average group velocity measurements for both (*AxiSEM* and *Mineos*) are centered around the first overtone value, but we see that the $\pm 1\sigma$ of calculated center frequency dependent group velocity also overlaps with the fundamental mode (Figure 4).

Figure 4. Data points: calculated group velocities from the mean times of the peaks of the envelopes of the filtered seismograms; averaged over a range of distances: 25°–150° epicentral distance, and center frequencies: 3–100 mHz. Also denoted is one standard deviation (1σ, normalized to N-1) of the samples. Overlaid fundamental mode and first overtone theoretical *Mineos* dispersion curves from *PlanetProfile* velocity models: (a) 0 km methane clathrate lid (pure water 100 km ice shell), (b) 10 km methane clathrate lid ice shell, and (c) 20 km methane clathrate lid ice shell. Also it is important to note that we denote *Mineos* and theoretical predictions and *AxiSEM* as mock observational measurements.

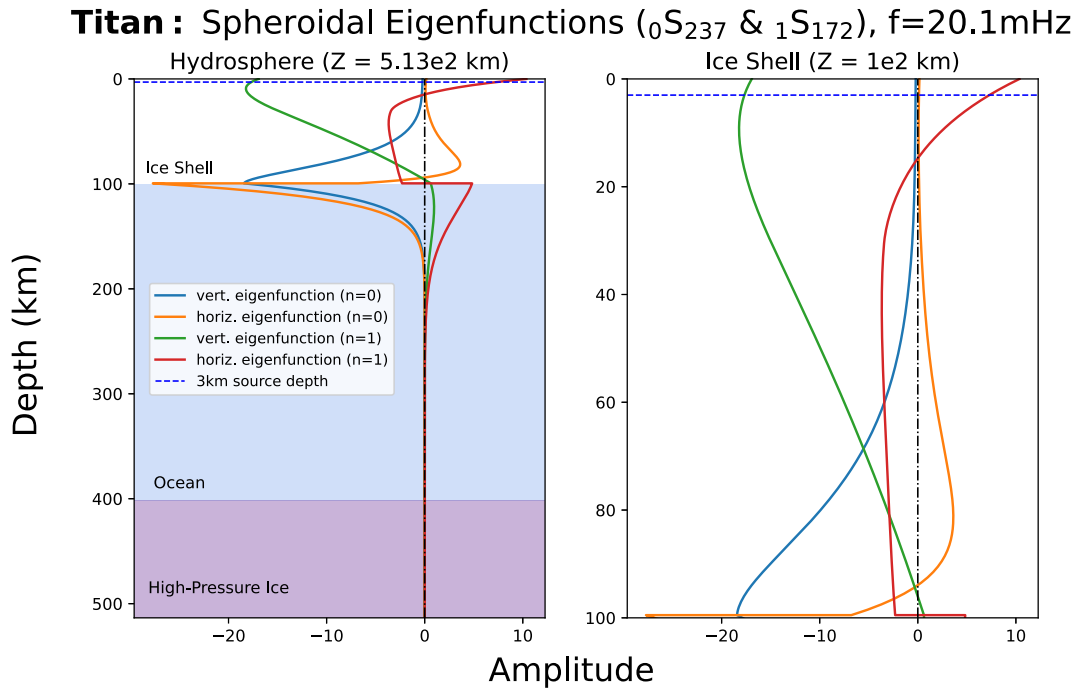

Figure 6. Vertical and horizontal eigenfunctions for a frequency of 20.1 mHz for both the fundamental mode ($n = 0, l = 237$) and first overtone ($n = 1, l = 172$). Seen in the fundamental mode is the Stoneley mode with high amplitudes at the base of the ice shell, and in the first overtone the Rayleigh wave is shown ($n = 1$). On the left side is the full Titan hydrosphere (total thickness of 513 km, including the ice shell, ocean, and underlying high pressure ice). On the right side the is a 100 km Titan ice shell in greater detail. The blue dashed line is plotted at 3 km depth, where the source in this study and Marusiak et al. (2022) is located.

Comparing the band-passed filtered seismograms (between 20 and 100 mHz) of the *AxiSEM/Instaseis* and normal mode summation generated *Mineos* models, the pure water ice shell and the 20 km clathrate lid model are the most similar, and the 10 km clathrate lid has the overall lowest amplitude (Figure 3). This is due to the thermal profiles of the models; the pure water ice shell and the 20 km clathrate lid models have the most similar thermal profiles, due to the stagnant lid thickness being similar, whereas the 10 km clathrate lid has the smallest conductive lid (Kalousová & Sotin, 2020; Marusiak et al., 2022) (Figure 7). The conductive, stagnant lid thickness plays a major role in the seismic amplitudes, as it influences the seismic attenuation (and its inverse, seismic quality factor), driving the amplitude differences between the Rayleigh wave (the most prominent feature in the seismograms) that we see in all of the models (Marusiak et al. (2022); this study: Figures 5 and 3). The Rayleigh wave can be seen in the first overtone, as opposed to the fundamental mode which was the expected dominant mode for dispersion measurements (Panning et al., 2006; Stähler et al., 2018).

We see clear separation of the mode information with the fundamental mode displaying the flexural wave at very low frequencies, below ≈3 mHz. The first overtone carries the high amplitude Rayleigh wave above ≈ 14 mHz (Figure 5). In Figure 5, in line with Figure 2, we have denoted the areas of the seismogram where the Rayleigh wave (first overtone) is dominant, and likewise for the flexural wave (fundamental mode) for a 25° seismogram (Table 1, Figure 3).

To understand the contributions that individual normal modes have on the resulting surface waves, we look at the individual normal mode seismograms (Figure 5) with *Mineos*, as well as plot the eigenfunctions (Equation 1). For all models, the fundamental mode peaks about 200s after the peak of the full normal mode (up to $n = 999$) seismogram (Figure 5). It is clear that the first overtone, rather than the fundamental mode, contains the Rayleigh wave energy at higher frequencies (Figures 2, 5 and 6). This is in agreement with the theoretical group velocity and is further confirmed by the eigenfunctions, where in the first overtone at 20.1 mHz within the ice shell we see the characteristic zero crossing of the horizontal eigenfunction, as well as the decay to zero within the ocean of the vertical eigenfunction (Figure 6). Meanwhile, the fundamental mode eigenfunction shows the characteristic peak

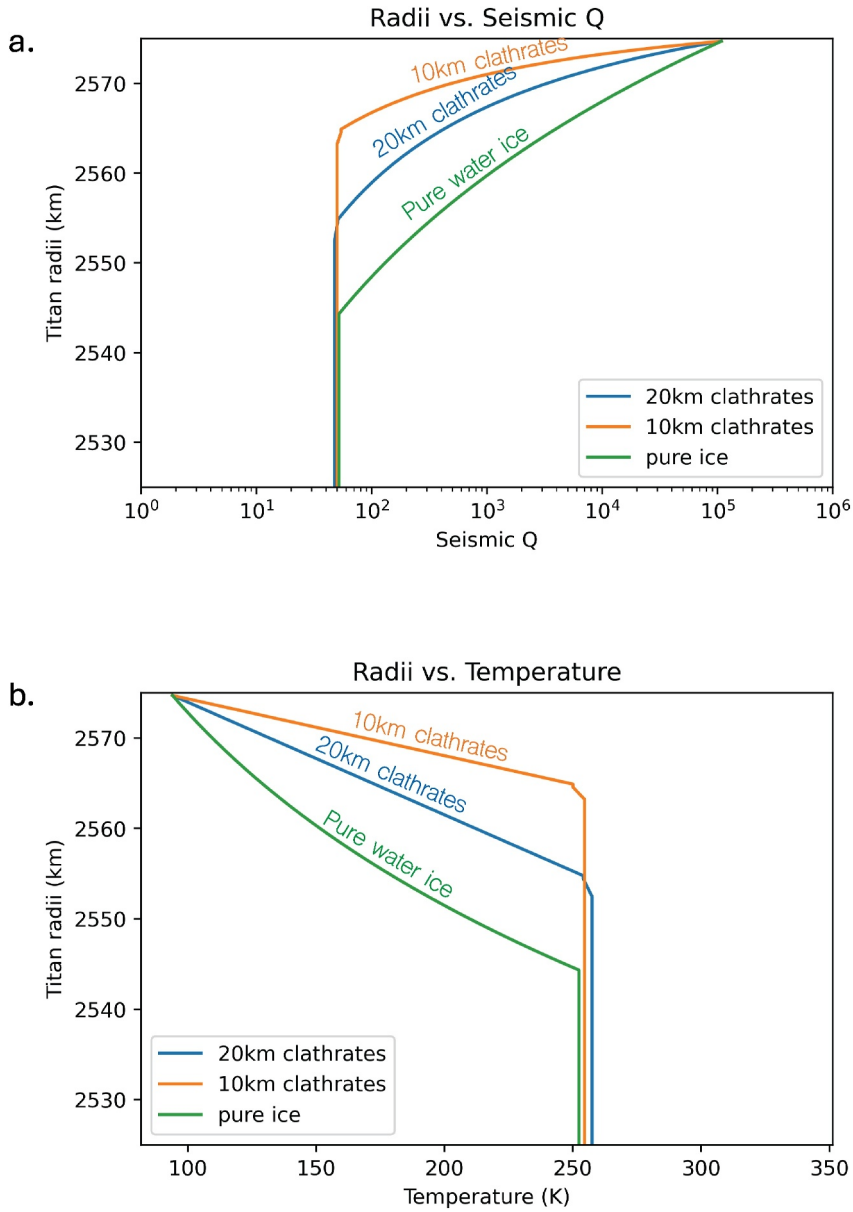

Figure 7. Plots of (a) radius versus seismic attenuation (quality factor-Q), and (b) radius versus the temperature for all models: pure water ice (no clathrates), 10 and 20 km methane clathrate-lids.

at the ice-ocean interface expected for a Stonely mode (Figure 6). Because the seismic source is shallow (3 km depth) the first overtone is excited instead of the fundamental mode, as the fundamental mode is a Stoneley mode excitable (and detectable) only for deep sources and receivers near the boundary of the ice shell and the subsurface ocean.

Taking a closer look at the eigenfunctions, we see vertical and horizontal motions of the long period flexural wave in the fundamental mode. At a frequency of 1.86 mHz, the flexural wave is the dominant surface wave seen in the ground displacement seismograms. The near constant vertical motion is seen in the blue in the vertical eigenfunction, decaying to zero in the ocean. Seen in the horizontal eigenfunction, is the oscillating compression and extension, the characteristic motion of the entire flexing of the ice shell (Figure 8).

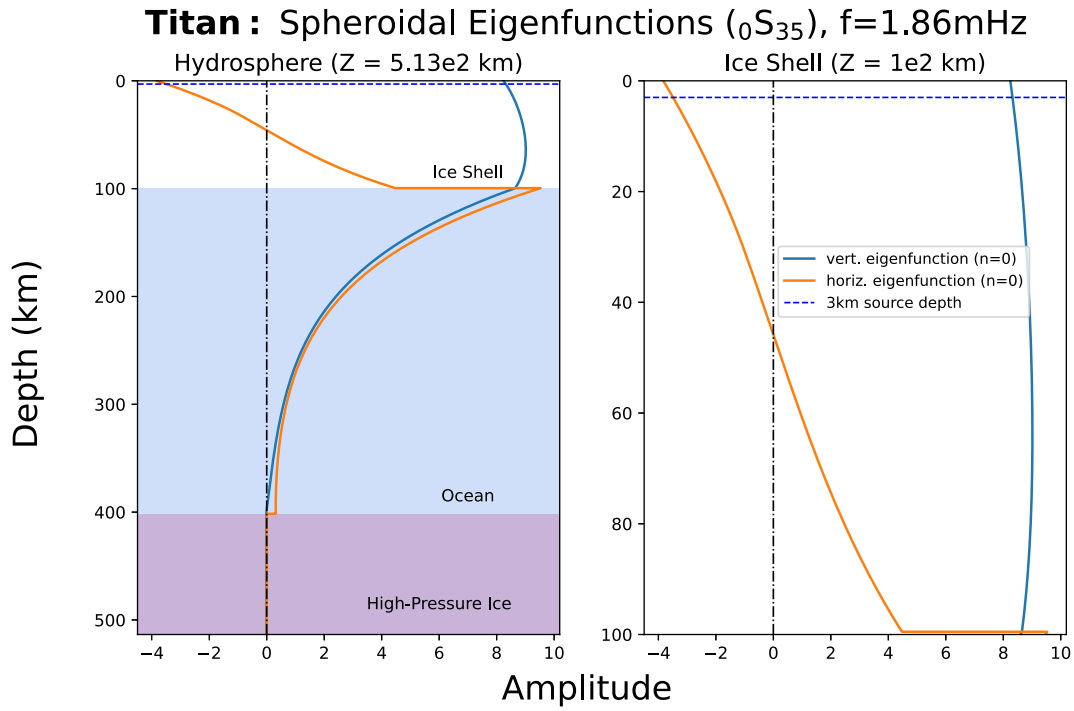

Figure 8. Vertical and horizontal eigenfunction amplitudes for the entire hydrosphere (region from the surface to the top of the mantle) at 1.86 mHz, for the fundamental mode where the flexural wave is the dominant feature ($n = 0, l = 35$). The model shown is a pure water 100 km, Titan ice shell. As in Figure 6, the blue dashed line at 3 km represents the depth of the source used in this study and Marusiak et al. (2022), with the complete Titan hydrosphere on the left panel, and the 100 km ice shell on the right panel.

4. Discussion

Our models are the same as Marusiak et al. (2022), with an additional 20 km clathrate model, which actually serves as an intermediary model given that it has a thicker stagnant lid/conductive region than the thinner 10 km clathrate model, and thus its thermal profile is more similar to the pure water ice shell. The thermal profile has implications for the seismic attenuation based on the choice of the thermodynamic model chosen for this study from Kalousová and Sotin (2020). Newer models have been released (Carnahan et al., 2022) that demonstrate more clathrate convection models—including models with clathrates at the bottom of the ice shell which could have large consequences for the thermal profile of the ice shell and chemical composition of the ocean.

To build off Marusiak et al. (2022), we study long-period/surface-wave seismology to investigate measurable differences that enable seismic data to constrain the presence and thickness of a clathrate lid. On a larger scale of analyzing interior models, the possible advantage of using long-period seismology, especially in the case of a single-station seismometer, is that it could enable direct resolution of the ice shell thickness better than using body-wave seismology alone, particularly in the event that we are not able to clearly identify body waves but have large amplitude surface waves, for example, (Panning et al., 2006). Maguire et al. (2021) found, at least in the case of flexural wave dispersion, thicker ice shells require extremely sensitive broadband seismometers. In the case of Europa, using group velocity measurements with periods of 25–250 s (frequencies ranging from 0.004 to 0.04 Hz) we can infer Europa's ice shell thickness using the Bayesian inversion method implemented by (Maguire et al., 2021). But it is important to note that the ability to constrain the ice shell thickness becomes steadily more inaccurate when using events from large epicentral distances. Europa also has an ice shell estimated to be 5–30 km (Schubert et al., 2004), a fraction of Titan's estimated ice shell thickness 25–200 km (Baland et al., 2014; Barnes et al., 2021; Béghin et al., 2012; Deschamps et al., 2010; Durante et al., 2019; Hemingway et al., 2013; Iess et al., 2012; Mitri & Showman, 2008; Nimmo & Bills, 2010; Sohl et al., 2014; Tobie et al., 2006). The thicker ice shell shifts relevant flexural wave signals to lower frequencies ($\lesssim \approx 2mHz$), increasing the challenge of measuring the relevant surface waves with a less sensitive seismometer such as that proposed for *Dragonfly*. *Dragonfly* will host a seismometer similar to the Lunar-A seismometer (Yamada et al., 2015), which has a peak

sensitivity around 1–2 Hz (Panning et al., 2020), more suited for detecting body wave signals. In order to increase the frequency sensitivity to long-period surface waves, it would require a more sensitive (and therefore more massive) seismometer, such as the broadband *InSight* VBB seismometer (Lognonné et al., 2019).

There are several sources of uncertainty for using surface waves to determine the ice shell thickness. The interior models used in this study are spherically symmetric which is simplified when compared to reality. Repeating this study in a heterogeneous, three-dimensional interior model,for example, (Marusiak et al., 2023), with added noise model could yield more realistic, Titan-like results. However, modeling in three dimensions on a global scale, and adding in complex noise sources are computationally expensive and non-uniquely determined, although it may be important in the future to adequately model real Titan data. For this study, we choose to investigate differences in surface waves under a simplified scenario. Additionally, we did not account for a realistic Titan noise environment or model instrument self-noise which would create additional challenges in measuring surface wave dispersion.

We see that the dispersion measurements are dominated by the first overtone. The uncertainties (1σ) of our measurements are greater than the variation of the group velocities for each model at various distances and frequencies. Thus we are unable to use surface wave dispersion to distinguish clathrate models from one another based upon the current simulated models (spherically symmetric Titan models, 100 km thick iceshells with and without methane-clathrate lids with a 10% magnesium sulfate ocean) (Figure 4). The uncertainties seen are inherent to making group velocity measurements on envelope data at a single station, which is the most likely measurement approach expected to be reliable on difficult planetary seismic data. Higher-precision group and phase velocity measurements can be achieved with more complex waveform modeling approaches, but this may not be possible on Titan with the single-station measurements from *Dragonfly* which relies on an instrument peaked at much higher frequencies. It's possible that source array approaches could be applied if there are multiple well-located events on Titan, but that will be difficult with a single vertical component seismometer and relatively noisy horizontal motions from geophones on the skids of the spacecraft.

While mode-stripping approaches to separate fundamental and higher mode branches may be possible with very high-quality seismic data, separating modes is likely to be quite challenging, particularly if the signal-to-noise ratio is not particularly high and epicentral distance is not well-constrained. Given these limitations expected in the real data, we chose to focus on measurements of group velocity on envelopes which is one of the most robust techniques possible in non-ideal measurement settings.

Analyzing signals in the context of expected signal and noise strength on Titan with *Dragonfly* is upcoming work, but both expected signal strength and environmental noise levels are not well-known. For this reason, we chose to focus in this study on simple approaches applied on noise-free data to understand limits on resolvability of structure in a reasonably best-case scenario. Additionally, a characterization of an ice cracking event on Titan has not been addressed in work or in any other previous works currently—but would make for a useful future paper. Estimates from Hurford et al. (2020) suggest that global cumulative seismic moment release per tidal cycle and maximum event size comparable to a $M_w = 5$ event could be expected on Titan, which could imply regular $M_w = 3$ events, but this is very difficult to constrain before arrival on Titan. Future work specifically modeling signal and noise strength comparable to existing work for Europa (Panning et al., 2018) is a likely topic for future study.

Future investigations of using long period seismology to investigate icy ocean worlds that could contain clathrates might consider looking at worlds with thinner ice shells (e.g., Europa or Enceladus). For example (Panning et al., 2006), used the multiple filter technique (MFT) (Dziewonski et al., 1969) to extract group velocity curves from a single measurement, even in the absence of location and absolute velocity information. However (Panning et al., 2006), also showed that when using this MFT method for flexural or Rayleigh wave propagation, error estimation increases with ice shell thickness. The frequency of the distinctive peak changes very little for ice shells greater than 40 km.

There are remaining discrepancies between the *AxiSEM/Instaseis* seismograms in comparison to *Mineos* (Figure 3). Ideally, both methods of generating seismograms should agree, especially since both use the same radial velocity profiles generated by *PlanetProfile*. The *AxiSEM/Instaseis* method uses Green's functions in the time domain, while *Mineos* uses normal mode summation in the frequency domain. We see that the seismograms are in phase, but not exactly identical in amplitude. Here we look at the ground motion velocity instead of the displacement, as data collected with the *Dragonfly* seismometer will be used to infer surface wave velocities. It is

possible that differences arise from poor numerical resolution of the mode calculations within *Mineos*, which is highly tuned for performance in Earth-like models, as demonstrated by the difficulty in calculating modes at frequencies greater than 150 mHz, the upper limit used in this study. However, we do see that both methods do show a great deal of consistency, as there is good agreement in calculating the group velocities (Figure 4).

Looking again at the ground displacement plots (Figure 4), we can see the flexural wave clearly in the fundamental mode. However, given real seismic data the *Dragonfly* seismometer will not be sensitive to this lower frequency ($\approx \geq 2$ mHz) information nearly three orders of magnitude below the peak sensitivity of the seismogram. Visualizing this modal decoupling in this manner (i.e., looking at the fundamental mode, first and second overtone, in comparison to the full mode summation) is more useful in pinpointing why this phenomenon (the Rayleigh pulse occurring in the first overtone, as opposed to the fundamental mode) occurs when there is a thick ice shell.

5. Conclusions

While *Mineos* dispersion predictions suggest differences between clathrate models, these differences are smaller than the uncertainty of the measurements we were able to make on synthetic data in this study. Thus we predict it would be difficult to detect clathrates lids using long period seismology on Titan. Of course this does not preclude using long period seismology at all on Titan, just further investigations of features in the ice would have to be conducted.

Future studies could include investigating clathrates at different depths, varying the composition of the ocean, or adding heterogeneities to the ice shell. Although these additions will only complicate the seismograms more, they will also make them more realistic for the comparison to real seismic data that will be received from *Dragonfly* in the mid-2030s. This research also applies to other icy ocean worlds where surface/near-surface clathrates could exist.

Data Availability Statement

The *PlanetProfile* v1.2.0 interior structure models (generated with MATLAB) are available on Github (https://github.com/vancesteven/PlanetProfile). The open source software packages, *AxiSEM* v1.3 (Nissen-Meyer et al., 2014), *Instaseis* (van Driel et al., 2015), *Mineos* v1.0.2 (Masters et al., 2011), and *TauP* (http://www.seis.sc.edu/TauP/) (Crotwell et al., 1999) are all open source and available for download. Interior structure models will be made available on NASA's Open Data Portal.

Acknowledgments
The authors would like to thank the *Dragonfly* Guest Investigator Program, members of the Jet Propulsion Laboratory's Moons Geology and Geophysics group especially Marshall Styczinski and Steve Vance. A. Bryant thanks Steve Meyer and Sunny Park at the University of Chicago for many helpful conversations. A part of the research was carried out at the Jet Propulsion Laboratory, California Institute of Technology, under a contract with the National Aeronautics and Space Administration (80NM0018D0004). A. Bryant was also funded partially by the *Dragonfly* Guest Investigator Program through the Johns Hopkins Applied Physics Laboratory.

References

Baland, R.-M., Tobie, G., Lefèvre, A., & Van Hoolst, T. (2014). Titan's internal structure inferred from its gravity field, shape, and rotation state. *Icarus*, *237*, 29–41. https://doi.org/10.1016/j.icarus.2014.04.007

Banerdt, W. B., Smrekar, S. E., Banfield, D., Giardini, D., Golombek, M., Johnson, C. L., et al. (2020). Initial results from the insight mission on mars. *Nature Geoscience*, *13*(3), 183–189. https://doi.org/10.1038/s41561-020-0544-y

Barnes, J. W., Brown, R. H., Soderblom, L., Buratti, B. J., Sotin, C., Rodriguez, S., et al. (2007). Global-scale surface spectral variations on titan seen from cassini/vims. *Icarus*, *186*(1), 242–258. https://doi.org/10.1016/j.icarus.2006.08.021

Barnes, J. W., Turtle, E. P., Trainer, M. G., Lorenz, R. D., MacKenzie, S. M., Brinckerhoff, W. B., et al. (2021). Science goals and objectives for the dragonfly titan rotorcraft relocatable lander. *The Planetary Science Journal*, *2*(4), 130. https://doi.org/10.3847/PSJ/abfdcf

Beghein, C., Li, J., Weidner, E., Maguire, R., Wookey, J., Lekic, V., et al. (2022). Crustal anisotropy in the martian lowlands from surface wave. *Geophysical Research Letters*, *49*(24), e2022GL101508. https://doi.org/10.1029/2022GL101508

Béghin, C., Randriamboarison, O., Hamelin, M., Karkoschka, E., Sotin, C., Whitten, R. C., et al. (2012). Analytic theory of titan's schumann resonance: Constraints on ionospheric conductivity and buried water ocean. *Icarus*, *218*(2), 1028–1042. https://doi.org/10.1016/j.icarus.2012.02.005

Carnahan, E., Vance, S. D., Hesse, M. A., Journaux, B., & Sotin, C. (2022). Dynamics of mixed clathrate-ice shells on ocean worlds. *Geophysical Research Letters*, *49*(8), e2021GL097602. https://doi.org/10.1029/2021GL097602

Choukroun, M., Grasset, O., Tobie, G., & Sotin, C. (2010). Stability of methane clathrate hydrates under pressure: Influence on outgassing processes of methane on Titan. *Icarus*, *205*(2), 581–593. https://doi.org/10.1016/j.icarus.2009.08.011

Cordiner, M. A., Nixon, C. A., Charnley, S. B., Teanby, N. A., Molter, E. M., Kisiel, Z., & Vuitton, V. (2018). Interferometric imaging of titan's hc3n, h13cccn, and hccc15n. *The Astrophysical Journal Letters*, *859*(1), L15. https://doi.org/10.3847/2041-8213/aac38d

Cordiner, M. A., Palmer, M. Y., Nixon, C. A., Irwin, P. G. J., Teanby, N. A., Charnley, S. B., et al. (2015). Ethyl cyanide on titan: Spectroscopic detection and mapping using alma. *The Astrophysical Journal Letters*, *800*(1), L14. https://doi.org/10.1088/2041-8205/800/1/L14

Crotwell, H. P., Owens, T. J., & Ritsema, J. (1999). The taup toolkit: Flexible seismic travel-time and ray-path utilities. *Seismological Research Letters*, *70*(2), 154–160. https://doi.org/10.1785/gssrl.70.2.154

Deschamps, F., Mousis, O., Sanchez-Valle, C., & Lunine, J. I. (2010). The role of methanol in the crystallization of titan's primordial ocean. *The Astrophysical Journal*, *724*(2), 887–894. https://doi.org/10.1088/0004-637X/724/2/887

Drilleau, M., Beucler, É., Shi, J., Knapmeyer-Endrun, B., Garcia, R. F., Ansan, V., et al. (2023). Structure of the Martian crust below InSight from surface waves and body waves generated by nearby meteoroid impacts. *Geophysical Research Letters*, *50*(23), e2023GL104601. https://doi.org/10.1029/2023GL104601

Durante, D., Hemingway, D., Racioppa, P., Iess, L., & Stevenson, D. (2019). Titan's gravity field and interior structure after cassini. *Icarus*, *326*, 123–132. https://doi.org/10.1016/j.icarus.2019.03.003

Dybing, S. N., Ringler, A. T., Wilson, D. C., & Anthony, R. E. (2019). Characteristics and spatial variability of wind noise on near-surface broadband seismometers. *Bulletin of the Seismological Society of America*, *109*(3), 1082–1098. https://doi.org/10.1785/0120180227

Dziewonski, A., Bloch, S., & Landisman, M. (1969). A technique for the analysis of transient seismic signals. *Bulletin of the Seismological Society of America*, *59*(1), 427–444. https://doi.org/10.1785/BSSA0590010427

Elachi, C., Wall, S., Allison, M., Anderson, Y., Boehmer, R., Callahan, P., et al. (2005). Cassini radar views the surface of titan. *Science*, *308*(5724), 970–974. https://doi.org/10.1126/science.1109919

Fortes, A. (2012). Titan's internal structure and the evolutionary consequences. *Planetary and Space Science*, *60*(1), 10–17. (Titan Through Time: A Workshop on Titan's Formation, Evolution and Fate). https://doi.org/10.1016/j.pss.2011.04.010

Grasset, O., Sotin, C., & Deschamps, F. (2000). On the internal structure and dynamics of titan. *Planetary and Space Science*, *48*(7–8), 617–636. https://doi.org/10.1016/S0032-0633(00)00039-8

Gutenberg, B. (1947). Microseisms and weather forecasting. *Journal of the Atmospheric Sciences*, *4*(1), 21–28. https://doi.org/10.1175/1520-0469(1947)004%3C0021:MAWF%3E2.0.CO;2

Hand, K. P., Chyba, C. F., Carlson, R. W., & Cooper, J. F. (2006). Clathrate hydrates of oxidants in the ice shell of Europa. *Astrobiology*, *6*(3), 463–482. https://doi.org/10.1089/ast.2006.6.463

Hayes, A. G. (2016). The lakes and seas of titan. *Annual Review of Earth and Planetary Sciences*, *44*(1), 57–83. https://doi.org/10.1146/annurev-earth-060115-012247

Hayes, A. G., Lorenz, R. D., & Lunine, J. I. (2018). A post-Cassini view of Titan's methane-based hydrologic cycle. *Nature Geoscience*, *11*(5), 306–313. https://doi.org/10.1038/s41561-018-0103-y

Hayne, P. O., McCord, T. B., & Sotin, C. (2014). Titan's surface composition and atmospheric transmission with solar occultation measurements by cassini vims. *Icarus*, *243*, 158–172. https://doi.org/10.1016/j.icarus.2014.08.045

Helgerud, M. B., Waite, W. F., Kirby, S. H., & Nur, A. (2003). Measured temperature and pressure dependence of Vp and vs in compacted, polycrystalline sI methane and sII methane-ethane hydrate. *Canadian Journal of Physics*, *81*(1–2), 47–53. https://doi.org/10.1139/p03-016

Helgerud, M. B., Waite, W. F., Kirby, S. H., & Nur, A. (2009). Elastic wave speeds and moduli in polycrystalline ice Ih, sI methane hydrate, and sII methane-ethane hydrate. *Journal of Geophysical Research*, *114*(B2), B02212. https://doi.org/10.1029/2008JB006132

Hemingway, D., Nimmo, F., Zebker, H., & Iess, L. (2013). A rigid and weathered ice shell on titan. *Nature*, *500*(7464), 550–552. https://doi.org/10.1038/nature12400

Hörst, S. M. (2017). Titan's atmosphere and climate. *Journal of Geophysical Research: Planets*, *122*(3), 432–482. https://doi.org/10.1002/2016JE005240

Hurford, T., Henning, W., Maguire, R., Lekic, V., Schmerr, N., Panning, M., et al. (2020a). Seismicity on tidally active solid-surface worlds. *Icarus*, *338*, 113466. https://doi.org/10.1016/j.icarus.2019.113466

Hurford, T. A., Henning, W., Maguire, R., Lekic, V., Schmerr, N. C., Panning, M. P., et al. (2020b). Seismicity on tidally active solid-surface worlds. *Icarus*, *338*, 113466. https://doi.org/10.1016/j.icarus.2019.113466

Iess, L., Jacobson, R. A., Ducci, M., Stevenson, D. J., Lunine, J. I., Armstrong, J. W., et al. (2012). The tides of titan. *Science*, *337*(6093), 457–459. https://doi.org/10.1126/science.1219631

Iess, L., Stevenson, D. J., Parisi, M., Hemingway, D., Jacobson, R. A., Lunine, J. I., et al. (2014). The gravity field and interior structure of enceladus. *Science*, *344*(6179), 78–80. https://doi.org/10.1126/science.1250551

Janssen, M., Le Gall, A., Lopes, R., Lorenz, R., Malaska, M., Hayes, A., et al. (2016). Titan's surface at 2.18-cm wavelength imaged by the cassini radar radiometer: Results and interpretations through the first ten years of observation. *Icarus*, *270*, 443–459. https://doi.org/10.1016/j.icarus.2015.09.027

Janssen, M., Lorenz, R., West, R., Paganelli, F., Lopes, R., Kirk, R., et al. (2009). Titan's surface at 2.2-cm wavelength imaged by the cassini radar radiometer: Calibration and first results. *Icarus*, *200*(1), 222–239. https://doi.org/10.1016/j.icarus.2008.10.017

Jennings, D., Cottini, V., Nixon, C., Achterberg, R., Flasar, F., Kunde, V., et al. (2016). Surface temperatures on titan during northern winter and spring. *The Astrophysical Journal Letters*, *816*(1), L17. https://doi.org/10.3847/2041-8205/816/1/L17

Journaux, B., Brown, J. M., Pakhomova, A., Collings, I. E., Petitgirard, S., Espinoza, P., et al. (2020). Holistic approach for studying planetary hydrospheres: Gibbs representation of ices thermodynamics, elasticity, and the water phase diagram to 2,300 mpa. *Journal of Geophysical Research: Planets*, *125*(1), e2019JE006176. https://doi.org/10.1029/2019JE006176

Kalousová, K., & Sotin, C. (2020). Dynamics of Titan's high-pressure ice layer. *Earth and Planetary Science Letters*, *545*, 116416. https://doi.org/10.1016/j.epsl.2020.116416

Khan, A., Ceylan, S., van Driel, M., Giardini, D., Lognonné, P., Samuel, H., et al. (2021). Upper mantle structure of mars from insight seismic data. *Science*, *373*(6553), 434–438. https://doi.org/10.1126/science.abf2966

Kim, D., Banerdt, W. B., Ceylan, S., Giardini, D., Lekić, V., Lognonné, P., et al. (2022). Surface waves and crustal structure on Mars. *Science*, *378*(6618), 417–421. https://doi.org/10.1126/science.abq7157

Kim, D., Duran, C., Giardini, D., Plesa, A.-C., Stähler, S. C., Boehm, C., et al. (2023). Global crustal thickness revealed by surface waves orbiting Mars. *Geophysical Research Letters*, *50*(12), e2023GL103482. https://doi.org/10.1029/2023GL103482

Knapmeyer-Endrun, B., Panning, M. P., Bissig, F., Joshi, R., Khan, A., Kim, D., et al. (2021). Thickness and structure of the martian crust from insight seismic data. *Science*, *373*(6553), 438–443. https://doi.org/10.1126/science.abf8966

Kovach, R. L., & Chyba, C. F. (2001). Seismic detectability of a subsurface ocean on Europa. *Icarus*, *150*(2), 279–287. https://doi.org/10.1006/icar.2000.6577

Lai, J. C.-Y., Cordiner, M. A., Nixon, C. A., Achterberg, R. K., Molter, E. M., Teanby, N. A., et al. (2017). Mapping vinyl cyanide and other nitriles in titan's atmosphere using alma. *The Astronomical Journal*, *154*(5), 206. https://doi.org/10.3847/1538-3881/aa8eef

Lebreton, J. P., Coustenis, A., Lunine, J., Raulin, F., Owen, T., & Strobel, D. (2009). Results from the huygens probe on titan. *Astronomy and Astrophysics Review*, *17*(2), 149–179. https://doi.org/10.1007/s00159-009-0021-5

Le Mouélic, S., Paillou, P., Janssen, M. A., Barnes, J. W., Rodriguez, S., Sotin, C., et al. (2008). Mapping and interpretation of sinlap crater on titan using cassini vims and radar data. *Journal of Geophysical Research*, *113*(E4). https://doi.org/10.1029/2007JE002965

Li, J., Beghein, C., Panning, M. P., Davis, P., Lognonné, P., Banerdt, W. B., et al. (2022). Different martian crustal seismic velocities across the dichotomy boundary from multi-orbiting surface waves. *Geophysical Research Letters*, *49*(1), e2022GL101243. https://doi.org/10.1029/2022GL101243

Lognonné, P., Banerdt, W. B., Giardini, D., Pike, W. T., Christensen, U., Laudet, P., et al. (2019). Seis: Insight's seismic experiment for internal structure of mars. *Space Science Reviews*, *215*(1), 12. https://doi.org/10.1007/s11214-018-0574-6
Lopes, R. M., Mitchell, K. L., Wall, S. D., Mitri, G., Janssen, M., Ostro, S., et al. (2007). The lakes and seas of titan. *EOS, Transactions American Geophysical Union*, *88*(51), 569–570. https://doi.org/10.1029/2007EO510001
Lopes, R. M. C., Wall, S. D., Elachi, C., Birch, S. P. D., Corlies, P., Coustenis, A., et al. (2019). Titan as revealed by the cassini radar. *Space Science Reviews*, *215*(4), 33. https://doi.org/10.1007/s11214-019-0598-6
Lorenz, R. D., & Le Gall, A. (2020). Schumann resonance on titan: A critical re-assessment. *Icarus*, *351*, 113942. https://doi.org/10.1016/j.icarus.2020.113942
Lorenz, R. D., MacKenzie, S. M., Neish, C. D., Le Gall, A., Turtle, E. P., Barnes, J. W., et al. (2021). Selection and characteristics of the dragonfly landing site near Selk crater, Titan. *Planetary Science Journal*, *2*(1), 24. https://doi.org/10.3847/PSJ/abd08f
Lorenz, R. D., Shiraishi, H., Panning, M., & Sotzen, K. (2021). Wind and surface roughness considerations for seismic instrumentation on a relocatable lander for Titan. *Planetary and Space Science*, *206*, 105320. https://doi.org/10.1016/j.pss.2021.105320
Lorenz, R. D., Turtle, E. P., Barnes, J. W., Trainer, M. G., Adams, D. S., & Hibbard, K. E. (2018). Dragonfly: A rotorcraft lander concept for scientific exploration at titan. *Johns Hopkins APL Technical Digest*, *34*(3), 14.
Lunine, J. I., & Stevenson, D. J. (1985). Thermodynamics of clathrate hydrate at low and high pressures with application to the outer solar system. *The Astrophysical Journal - Supplement Series*, *58*(3), 493–531. https://doi.org/10.1086/191050
Lunine, J. I., & Stevenson, D. J. (1987). Clathrate and ammonia hydrates at high pressure: Application to the origin of methane on Titan. *Icarus*, *70*(1), 61–77. https://doi.org/10.1016/0019-1035(87)90075-3
Maguire, R. R., Schmerr, N. C., Lekić, V., Hurford, T. A., Dai, L., & Rhoden, A. R. (2021). Constraining Europa's ice shell thickness with fundamental mode surface wave dispersion. *Icarus*, *369*, 114617. https://doi.org/10.1016/j.icarus.2021.114617
Marusiak, A. G., Tharimena, S., Panning, M. P., Vance, S. D., Boehm, C., Stähler, S., & Van Driel, M. (2023). Estimating the 3d structure of the enceladus ice shell from flexural and crary waves using seismic simulations. *Earth and Planetary Science Letters*, *603*, 117984. https://doi.org/10.1016/j.epsl.2022.117984
Marusiak, A. G., Vance, S., Panning, M. P., Běhounková, M., Byrne, P. K., Choblet, G., et al. (2021). Exploration of icy ocean worlds using geophysical approaches. *The Planetary Science Journal*, *2*(4), 150. https://doi.org/10.3847/psj/ac1272
Marusiak, A. G., Vance, S., Panning, M. P., Bryant, A. S., Hesse, M. A., Carnahan, E., & Journaux, B. (2022). The effects of methane clathrates on the thermal and seismic profile of titan's icy lithosphere. *The Planetary Science Journal*, *3*(7), 167. https://doi.org/10.3847/PSJ/ac787e
Masters, G., Woodhouses, J. H., & Freeman, G. (2011). Mineos. Computational infrastructure of geodynamics.
Mitri, G., & Showman, A. P. (2008). Thermal convection in ice-i shells of titan and enceladus. *Icarus*, *193*(2), 387–396. https://doi.org/10.1016/j.icarus.2007.07.016
Nakamura, Y., Latham, G. V., & Dorman, H. J. (1982). Apollo lunar seismic experiment—Final summary. *Lunar and Planetary Science Conference Proceedings*, *87*(S01), 117–A123. https://doi.org/10.1029/JB087iS01p0A117
Neish, C. D., Barnes, J. W., Sotin, C., MacKenzie, S., Soderblom, J. M., Le Mouélic, S., et al. (2015). Spectral properties of titan's impact craters imply chemical weathering of its surface. *Geophysical Research Letters*, *42*(10), 3746–3754. https://doi.org/10.1002/2015GL063824
Niemann, H. B., Atreya, S. K., Bauer, S. J., Carignan, G. R., Demick, J. E., Frost, R. L., et al. (2005). The abundances of constituents of titan's atmosphere from the gcms instrument on the huygens probe. *Nature*, *438*(7069), 779–784. https://doi.org/10.1038/nature04122
Nimmo, F., & Bills, B. (2010). Shell thickness variations and the long-wavelength topography of titan. *Icarus*, *208*(2), 896–904. https://doi.org/10.1016/j.icarus.2010.02.020
Nissen-Meyer, T., van Driel, M., Stähler, S. C., Hosseini, K., Hempel, S., Auer, L., et al. (2014). AxiSEM: Broadband 3-D seismic wavefields in axisymmetric media. *Solid Earth*, *5*(1), 425–445. https://doi.org/10.5194/se-5-425-2014
Nixon, C. A., Thelen, A. E., Cordiner, M. A., Kisiel, Z., Charnley, S. B., Molter, E. M., et al. (2020). Detection of cyclopropenylidene on titan with alma. *The Astronomical Journal*, *160*(5), 205. https://doi.org/10.3847/1538-3881/abb679
Nunn, C., Garcia, R. F., Nakamura, Y., Marusiak, A. G., Kawamura, T., Sun, D., et al. (2020). Lunar seismology: A data and instrumentation review. *Space Science Reviews*, *216*(5), 89. https://doi.org/10.1007/s11214-020-00709-3
Nunn, C., Nakamura, Y., Kedar, S., & Panning, M. P. (2022). A new archive of apollo's lunar seismic data. *The Planetary Science Journal*, *3*(9), 219. https://doi.org/10.3847/PSJ/ac87af
Panning, M. P., Banerdt, W. B., Beghein, C., Carrasco, S., Ceylan, S., Clinton, J. F., et al. (2023). Locating the largest event observed on Mars with multi-orbit surface waves. *Geophysical Research Letters*, *50*(1), e2022GL101270. https://doi.org/10.1029/2022GL101270
Panning, M. P., Lekic, V., Manga, M., Cammarano, F., & Romanowicz, B. (2006). Long-period seismology on Europa: 2. Predicted seismic response. *Journal of Geophysical Research*, *111*(E12). https://doi.org/10.1029/2006JE002712
Panning, M. P., Lorenz, R., Shiraishi, H., Yamada, R., Stähler, S., Turtle, E. P., et al. (2020). Seismology on titan: A seismic signal and noise budget in preparation for dragonfly. In *Seg international exposition and annual meeting* (p. D041S079R005). https://doi.org/10.1190/segam2020-3426937.1
Panning, M. P., Stähler, S. C., Huang, H. H., Vance, S. D., Kedar, S., Tsai, V. C., et al. (2018). Expected seismicity and the seismic noise environment of Europa. *Journal of Geophysical Research: Planets*, *123*(1), 163–179. https://doi.org/10.1002/2017JE005332
Porco, C. C., Helfenstein, P., Thomas, P. C., Ingersoll, A. P., Wisdom, J., West, R., et al. (2006). Cassini observes the active south pole of Enceladus. *Science*, *311*(5766), 1393–1401. https://doi.org/10.1126/science.1123013
Rodriguez, S., Le Mouélic, S., Sotin, C., Clénet, H., Clark, R., Buratti, B., et al. (2006). Cassini/vims hyperspectral observations of the huygens landing site on titan. *Planetary and Space Science*, *54*(15), 1510–1523. https://doi.org/10.1016/j.pss.2006.06.016
Schubert, G., Anderson, J., Spohn, T., & McKinnon, W. (2004). Interior composition, structure and dynamics of the galilean satellites. *Jupiter: The planet, satellites and magnetosphere*, *1*, 281–306.
Schurmeier, L. R., Dombard, A. J., Malaska, M. J., Fagents, S. A., Radebaugh, J., & Lalich, D. E. (2023). An intrusive cryomagmatic origin for northern radial labyrinth terrains on titan and implications for the presence of crustal clathrates. *Icarus*, *404*, 115664. https://doi.org/10.1016/j.icarus.2023.115664
Shearer, P. M. (2019). *Introduction to seismology* (3rd ed.). Cambridge University Press.
Soderblom, L. A., Kirk, R. L., Lunine, J. I., Anderson, J. A., Baines, K. H., Barnes, J. W., et al. (2007). Correlations between cassini vims spectra and radar sar images: Implications for titan's surface composition and the character of the huygens probe landing site. *Planetary and Space Science*, *55*(13), 2025–2036. https://doi.org/10.1016/j.pss.2007.04.014
Sohl, F., Hussmann, H., Schwentker, B., Spohn, T., & Lorenz, R. D. (2003). Interior structure models and tidal Love numbers of Titan. *Journal of Geophysical Research*, *108*(E12). https://doi.org/10.1029/2003JE002044
Sohl, F., Solomonidou, A., Wagner, F. W., Coustenis, A., Hussmann, H., & Schulze-Makuch, D. (2014). Structural and tidal models of titan and inferences on cryovolcanism. *Journal of Geophysical Research: Planets*, *119*(5), 1013–1036. https://doi.org/10.1002/2013JE004512

Sotin, C., Kalousová, K., & Tobie, G. (2021). Titan's interior structure and dynamics after the cassini-huygens mission. *Annual Review of Earth and Planetary Sciences*, *49*(1), 579–607. https://doi.org/10.1146/annurev-earth-072920-052847

Stähler, S. C., Khan, A., Banerdt, W. B., Lognonné, P., Giardini, D., Ceylan, S., et al. (2021). Seismic detection of the martian core. *Science*, *373*(6553), 443–448. https://doi.org/10.1126/science.abi7730

Stähler, S. C., Panning, M. P., Hadziioannou, C., Lorenz, R. D., Vance, S., Klingbeil, K., & Kedar, S. (2019). Seismic signal from waves on titan's seas. *Earth and Planetary Science Letters*, *520*, 250–259. https://doi.org/10.1016/j.epsl.2019.05.043

Stähler, S. C., Panning, M. P., Vance, S. D., Lorenz, R. D., van Driel, M., Nissen-Meyer, T., & Kedar, S. (2018). Seismic wave propagation in icy ocean worlds. *Journal of Geophysical Research: Planets*, *123*(1), 206–232. https://doi.org/10.1002/2017JE005338

Stofan, E. R., Elachi, C., Lunine, J. I., Lorenz, R. D., Stiles, B., Mitchell, K. L., et al. (2007). The lakes of Titan. *Nature*, *445*(7123), 61–64. https://doi.org/10.1038/nature05438

Styczinski, M. J., Vance, S. D., & Melwani Daswani, M. (2023). *PlanetProfile:* Self-consistent interior structure modeling for terrestrial bodies in python. *Earth and Space Science*, *10*(8), e2022EA002748. https://doi.org/10.1029/2022EA002748

Sun, Y., Zhao, J., Hou, C., & Jiao, W. (2023). Highlight advances in planetary physics in the solar system: In situ detection over the past 20 years. *Space: Science and Technology*, *3*, 0007. https://doi.org/10.34133/space.0007

Thelen, A. E., Cordiner, M. A., Nixon, C. A., Vuitton, V., Kisiel, Z., Charnley, S. B., et al. (2020). Detection of ch3c3n in titan's atmosphere. *The Astrophysical Journal Letters*, *903*(1), L22. https://doi.org/10.3847/2041-8213/abc1e1

Thelen, A. E., Nixon, C., Chanover, N., Cordiner, M., Molter, E., Teanby, N., et al. (2019). Abundance measurements of titan's stratospheric hcn, hc3n, c3h4, and ch3cn from alma observations. *Icarus*, *319*, 417–432. https://doi.org/10.1016/j.icarus.2018.09.023

Tobie, G., Grasset, O., Lunine, J. I., Mocquet, A., & Sotin, C. (2005). Titan's internal structure inferred from a coupled thermal-orbital model. *Icarus*, *175*(2), 496–502. https://doi.org/10.1016/j.icarus.2004.12.007

Tobie, G., Lunine, J. I., & Sotin, C. (2006). Episodic outgassing as the origin of atmospheric methane on titan. *Nature*, *440*(7080), 61–64. https://doi.org/10.1038/nature04497

Turtle, E., & Lorenz, R. (2021). The dragonfly mission to titan: Technological development and science converge to enable new exploration. *The Bridge*, *51*(3), 59–66.

Vance, S. D., Kedar, S., Panning, M. P., Stähler, S. C., Bills, B. G., Lorenz, R. D., et al. (2018a). Vital signs: Seismology of icy ocean worlds. *Astrobiology*, *18*(1), 37–53. https://doi.org/10.1089/ast.2016.1612

Vance, S. D., Panning, M. P., Stähler, S., Cammarano, F., Bills, B. G., Tobie, G., et al. (2018b). Geophysical investigations of habitability in ice-covered ocean worlds. *Journal of Geophysical Research: Planets*, *123*(1), 180–205. https://doi.org/10.1002/2017JE005341

van Driel, M., Krischer, L., Stähler, S. C., Hosseini, K., & Nissen-Meyer, T. (2015). Instaseis: Instant global seismograms based on a broadband waveform database. *Solid Earth*, *6*(2), 701–717. https://doi.org/10.5194/se-6-701-2015

Waite, W. F., Stern, L. A., Kirby, S. H., Winters, W. J., & Mason, D. H. (2007). Simultaneous determination of thermal conductivity, thermal diffusivity and specific heat in sI methane hydrate. *Geophysical Journal International*, *169*(2), 767–774. https://doi.org/10.1111/j.1365-246X.2007.03382.x

Woodhouse, J. H. (1988). *The calculation of eigenfrequencies and eigenfunctions of the free oscillations of the earth and the sun* (pp. 321–370). Seismological Algorithms.

Yamada, R., Nébut, T., Shiraishi, H., Lognonné, P., Kobayashi, N., & Tanaka, S. (2015). Frequency band enlargement of the penetrator seismometer and its application to moonquake observation. *Advances in Space Research*, *56*(2), 341–354. https://doi.org/10.1016/j.asr.2015.04.024